Geophysical Research Letters

RESEARCH LETTER
10.1029/2020GL089609

Key Points:

- A simple one-dimensional climate model exhibits a peak in equilibrium climate sensitivity (ECS) at a surface temperature of around 310 K
- This peak in ECS arises from a competition between decreasing emission from the H_2O "windows" and increasing emission from CO_2 "radiator fins"
- Moist-adiabatic warming in the upper troposphere is key for the efficacy of the CO_2 radiator fins, and hence for the ECS peak

Supporting Information:

- Supporting Information S1

Correspondence to:
J. T. Seeley,
jacob.t.seeley@gmail.com

Citation:
Seeley, J. T., & Jeevanjee, N. (2021). H_2O windows and CO_2 radiator fins: A clear-sky explanation for the peak in equilibrium climate sensitivity. *Geophysical Research Letters*, *48*, e2020GL089609. https://doi.org/10.1029/2020GL089609

Received 1 JUL 2020
Accepted 4 DEC 2020

H_2O Windows and CO_2 Radiator Fins: A Clear-Sky Explanation for the Peak in Equilibrium Climate Sensitivity

Jacob T. Seeley[1] **and Nadir Jeevanjee**[2]

[1]Harvard University Center for the Environment, Cambridge, MA, USA, [2]Geophysical Fluid Dynamics Laboratory, Princeton, NJ, USA

Abstract Recent explorations of the state-dependence of Earth's equilibrium climate sensitivity (ECS) have revealed a pronounced *peak* in ECS at a surface temperature of ∼310 K. This ECS peak has been observed in models spanning the model hierarchy, suggesting a robust physical source. Here, we propose an explanation for this ECS peak using a novel spectrally resolved decomposition of clear-sky longwave feedbacks. We show that the interplay between spectral feedbacks in H_2O-dominated and CO_2-dominated portions of the longwave spectrum, along with moist-adiabatic amplification of upper-tropospheric warming, conspire to produce a minimum in the feedback parameter, and a corresponding peak in ECS, at a surface temperature of 310 K. Mechanism-denial tests highlight three key ingredients for the ECS peak: (1) H_2O continuum absorption to quickly close spectral windows at high surface temperature; (2) moist-adiabatic tropospheric temperatures to enhance upper-tropospheric warming; and (3) energetically consistent increases of CO_2 with surface temperature.

Plain Language Summary Earth's equilibrium climate sensitivity (ECS) is roughly defined as the equilibrium change in surface temperature resulting from a doubling of CO_2. It is well-known that ECS can exhibit a considerable state-dependence, in that its value depends on both the baseline surface temperature and CO_2 concentration. Curiously, recent explorations of the state-dependence of ECS have revealed the presence of a pronounced peak in ECS at a surface temperature of ∼310 K, with ECS then decreasing at higher surface temperatures and CO_2 concentrations. Here, we propose an explanation for this peak in ECS that depends only on clear-sky longwave feedbacks. Our explanation attributes the peak in ECS to a minimum in the magnitude of the feedback parameter, which occurs as the system transitions between two different methods of reequilibrating to an imposed energy imbalance. At low surface temperature and CO_2, Earth reequilibrates to an imposed imbalance by changing the amount of radiation escaping to space through spectral windows where the opacity of H_2O is low. At high surface temperatures and CO_2 concentrations, these H_2O "windows" have closed, and Earth reequilibrates primarily by changing the amount of radiation escaping to space in spectral intervals where CO_2 opacity dominates over H_2O opacity.

1. Introduction

Earth's equilibrium climate sensitivity (ECS) is arguably the most studied quantity in climate science, with a history going back over 100 years and intensive study continuing to the present day (Arrhenius, 1896; Sherwood et al., 2020). ECS is defined as the equilibrium change in surface temperature resulting from a doubling of CO_2 relative to its preindustrial value, and is typically written using the forcing-feedback framework as

$$\mathrm{ECS} = \frac{F_{2x}}{\lambda_{\mathrm{eff}}}, \tag{1}$$

where F_{2x} is the radiative forcing from doubling CO_2 (in W/m^2) and λ_{eff} is the effective feedback parameter (in $W/m^2/K$), defined by Equation 1. (The forcing-feedback framework says that λ_{eff} can also be calculated via radiative perturbation calculations, a claim we verify below.)

Strictly speaking, ECS is defined only relative to a preindustrial base climate (Knutti et al., 2017). But this definition can be broadened to include other base climates, and when this is done ECS exhibits a

considerable *state-dependence*, in that its value varies with both baseline surface temperature and CO_2 concentration. This has been seen in global climate models as well as the paleoclimate record (Bloch-Johnson et al., 2015; Knutti & Rugenstein, 2015; Rohling et al., 2012, and references therein). In modeling studies, this state-dependence often takes the form of an increase in ECS with increasing surface temperature and CO_2. By Equation 1, this increase can be understood in terms of F_{2x} and λ_{eff}. In terms of forcing, it is understood that F_{2x} increases monotonically with surface temperature and CO_2, due to both increasing surface-atmosphere temperature contrast as well as increasing radiative efficacy of secondary CO_2 bands (Jeevanjee et al., 2020; Zhong & Haigh, 2013). In terms of feedbacks, a decrease in λ_{eff} (which increases ECS) would be expected from a strengthening water vapor feedback due to the closing of the water vapor spectral "windows" (e.g., Koll & Cronin, 2018). But, recent explorations of the state-dependence of ECS have revealed an even more curious phenomenon: a pronounced *peak* in ECS at a surface temperature T_s between about 310 and 320 K, with ECS then decreasing at higher T_s and CO_2 concentrations (Meraner et al., 2013; Popp et al., 2016; Romps, 2020; Russell et al., 2013; Wolf et al., 2018). The majority of these studies reported peak ECS values of roughly 6–8 K (although Wolf et al. (2018) and Popp et al. (2016) found significantly larger values in excess of 15 K).

This ECS peak has been observed in models spanning the model hierarchy, from single column models with minimal physics to comprehensive coupled GCMs with elaborate cloud and cumulus parameterizations. The proposed explanations for the peak vary accordingly, ranging from longwave clear-sky feedbacks (Meraner et al., 2013) to various cloud feedbacks (Russell et al., 2013; Wolf et al., 2018). While a diversity of feedbacks is likely involved, the ubiquity of the ECS peak suggests that a rather fundamental mechanism is at play, stemming from robust physics and not reliant on, say, the output of a particular cloud parameterization. Note that forcing is not a candidate for the ECS peak, as F_{2x} is monotonic in T_s and CO_2 (e.g., Caballero & Huber, 2013).

This state of affairs was highlighted in the recent work of Romps (2020), which studied cloud-resolving simulations of radiative-convective equilibrium (RCE) with a closed surface energy budget. Using a novel equilibration technique which allowed for a near-continuous exploration of a large range of CO_2 concentrations, Romps (2020) found a dramatic and well-resolved ECS peak, again in the neighborhood of 310 K. This peak was again attributed to a peak in λ_{eff}, not F_{2x}. Moreover, these simulations have small cloud fraction maxima (relative to GCMs) of roughly 10% or less, again pointing away from poorly constrained cloud feedbacks and toward something more fundamental.

These findings motivated us to search for an explanation for the ECS peak in terms of only clear-sky longwave feedbacks. Here, we propose such an explanation which relies only on the CO_2 and H_2O greenhouse effects, as well as the thermodynamics of moist adiabats, consistent with the analysis of Meraner et al. (2013). Our explanation rests on a novel *spectrally resolved* feedback decomposition, rather than the traditional decomposition of clear-sky feedbacks (i.e., Planck, lapse rate, and water vapor). As we will show, the interplay between spectral feedbacks in H_2O-dominated and CO_2-dominated portions of the longwave spectrum, along with moist-adiabatic amplification of temperature change in the upper troposphere, conspire to produce a pronounced minimum in λ_{eff} and a corresponding peak in ECS at a surface temperature of ∼310 K.

2. Methods

2.1. A Very Simple Climate Model

In this work, we study the ECS of a very simple 1-D RCE "climate model," in the spirit of the earliest climate models (e.g., Kluft et al., 2019; Manabe & Strickler, 1964) and guided by the principle of avoiding inessential complexity insofar as possible (Jeevanjee et al., 2017). Similar to many 1-D RCE models, we will focus on clear-sky physics and omit clouds (and hence cloud feedbacks) from our model. In contrast to earlier 1-D RCE calculations, however, we will not equilibrate T_s at fixed CO_2 using interactive shortwave and longwave radiation and a convective adjustment; instead, inspired by Romps (2020), we equilibrate the CO_2 *concentration* toward a specified value of the outgoing longwave radiation (OLR), keeping T_s fixed and imposing a moist-adiabatic temperature profile. By fixing the thermodynamic variables and equilibrating using longwave radiation only, we obviate the need for shortwave radiation entirely, as well as the need for

a convective adjustment (or any other form of convective parameterization). In these ways, our model is even simpler than the typical 1-D RCE model, and isolates longwave clear-sky physics as motivated above.

The detailed construction of our model is as follows: the thermal structure of the atmosphere is assumed to follow the pseudoadiabatic lapse rate in the troposphere, with an overlying isothermal stratosphere at a fixed tropopause temperature T_{tp} (Hartmann & Larson, 2002; Seeley et al., 2019). Relative humidity RH in the troposphere is assumed to be vertically uniform, and the H_2O mass fraction in the stratosphere is set equal to its value at the tropopause. Our default values for T_{tp} and RH are 200 K and 75%, respectively, approximating global-mean conditions; we test the sensitivity of our results to plausible changes in these values. The surface pressure is fixed at 101,325 Pa (therefore ignoring the roughly 3% increase in column mass from the increased CO_2 and H_2O at the upper end of our T_s range).

As mentioned above, our definition of an equilibrated climate state is based solely on OLR rather than the net (shortwave + longwave) flux at the top-of-atmosphere. To set the equilibrium value of OLR for a given experimental configuration (i.e., each combination of T_{tp}, RH, and any other varied parameters), we proceed as follows: we first calculate the OLR for a baseline simulation with $T_s = 288$ K and 280 ppm of CO_2, meant to roughly approximate the preindustrial global-mean climate. We call the resulting OLR value OLR_0, and use it as our equilibrium OLR value for other simulations with varied surface temperature. That is, for each other surface temperature under consideration, we adjust the CO_2 amount until the OLR is equal to OLR_0 (to within a precision of 10^{-2} W/m^2). This yields pairs of values of T_s and C, where C is the equilibrated CO_2 concentration. We carry out this procedure for surface temperatures between 280 and 325 K at 1-K increments. With the resulting set of (T_s, C) pairs we then construct, by piecewise-linear interpolation, continuous functions $T_s(C)$ and $C(T_s)$ (following Romps, 2020). Figure S1 shows $C(T_s)$ for our default configuration, which was equilibrated to $OLR_0 = 264.85$ W/m^2. With these functions in hand, we can then compute ECS at a given (T_s, C) as

$$\mathrm{ECS} = T_s(2C) - T_s(C). \tag{2}$$

Figure S1 shows the graphical interpretation of this procedure for calculating ECS.

Since there is no shortwave radiation in this model there is no surface albedo, hence no surface albedo feedback or shortwave water vapor feedback. The H_2O greenhouse effect and the thermodynamics of moist adiabats are included, however, so the usual water vapor and lapse-rate feedbacks are present, though they will not be diagnosed in the conventional way. Also, greenhouse gases besides CO_2 and H_2O are not considered; including preindustrial concentrations of methane or nitrous oxide changes our results only slightly (not shown), and ozone profiles are state-dependent and thus require interactive ozone chemistry which is beyond the scope of this study. (Future work could quantify the effect of ozone on the results shown here, e.g., Gómez-Leal et al., 2019). Also, since T_s is fixed and there is no convective parameterization, there is no need to consider surface enthalpy fluxes, although if desired their sum could be diagnosed as the integrated radiative cooling of our column.

2.2. Radiative Transfer Modeling

The radiative transfer calculations are the most complex aspect of our simple climate model. We used the Reference Forward Model (RFM) (Dudhia, 2017), a contemporary line-by-line code, to compute spectrally resolved OLR for the 1-D atmospheric soundings of our simple climate model. Our calculations cover the spectral range from 0 to 3,000 cm^{-1} with a resolution of $\Delta\nu = 0.1$ cm^{-1}, and our vertical grid extends from the surface to a height of 60 km with a vertical grid spacing of $\Delta z = 200$ m. We calculated radiative fluxes via the two-stream approximation with first-moment Gaussian quadrature (Clough et al., 1992). Our spectroscopic data were drawn from the latest version of the HITRAN database (Gordon et al., 2017); we used HITRAN data for all available isotopes of CO_2 and H_2O, weighted by their relative abundances (as is HITRAN convention). The RFM calculates atmospheric layer opacities on the user-supplied spectral grid by summing the contributions from all local lines with a lineshape truncation of 25 cm^{-1}. The RFM models the sub-Lorentzian far wings of CO_2 lines with the so-called χ-factor approach (Cousin et al., 1985), and continuum absorption is modeled with version 3.2 of the MTCKD code (Mlawer et al., 2012).

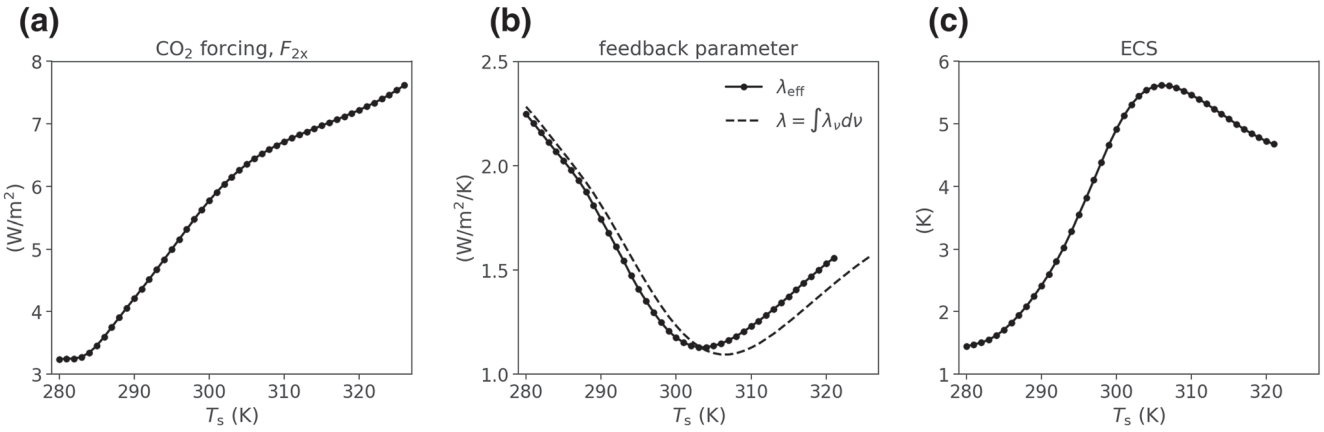

Figure 1. From the simple 1-D climate model, as a function of surface temperature T_s: (a) the radiative forcing from doubling CO_2 (Equation 3); (b) the effective feedback parameter λ_{eff} diagnosed from Equation 1, compared to the differential feedback parameter λ from Equation 4; (c) the equilibrium climate sensitivity (ECS, Equation 2).

3. Results

3.1. The Peak in ECS

The rightmost panel of Figure 1 plots ECS as a function of T_s from our simple climate model in its default configuration (with $T_{tp} = 200$ K and RH = 75%). For the preindustrial base state ($T_s = 288$ K), we obtain an ECS of about 2.1 K, at the low end of the IPCC range (IPCC, 2014). For warmer base states, ECS increases until it reaches a peak at approximately the same surface temperature (slightly below 310 K) as found by Romps (2020) in a cloud-resolving model, although our peak is not as sharp. The peak ECS value in our model (~5.5 K) is at the low end of the range found in most previous work (6–8 K). The existence of the ECS peak in our model is robust to reasonable changes in tropospheric RH and tropopause temperature T_{tp}, but the temperature at which the peak occurs is delayed by decreasing the RH, and vice versa (Figure S2).

As has been found in prior work (see Section 1), our peak in ECS is attributable to a minimum in λ_{eff} at nearly the same surface temperature (Figure 1b). We calculate λ_{eff} as F_{2x}/ECS (Equation 1), where F_{2x} is calculated at state (T_s, C) as

$$F_{2x} = \mathrm{OLR}(T_s, C) - \mathrm{OLR}(T_s, 2C). \tag{3}$$

Note that the first panel of Figure 1 confirms that F_{2x} is not a candidate explanation for the peak in ECS, as mentioned in Section 1.

Therefore, to explain the ECS peak, we must explain why λ_{eff} has a minimum. To this end, it is helpful to note that the effective feedback λ_{eff} can be approximated by the differential feedback parameter, λ, which is obtained not as F_{2x}/ECS but rather by incrementing the surface temperature by 1 K and taking a finite difference in OLR

$$\lambda = \frac{\mathrm{OLR}(T_s + 1, C) - \mathrm{OLR}(T_s, C)}{1\ \mathrm{K}}. \tag{4}$$

Note that when we increment the surface temperature by 1 K, we use the moist-adiabatic sounding associated with that warmer surface temperature, which means that the conventional lapse rate and fixed-RH water vapor feedbacks are included in the response. The middle panel of Figure 1 shows that $\lambda_{eff} \simeq \lambda$, validating the forcing-feedback framework. Since λ, unlike λ_{eff}, is computed as the OLR difference resulting from T_s-mediated changes in thermodynamic profiles, we can spectrally decompose it to better understand the impact of these thermodynamic changes on TOA radiation.

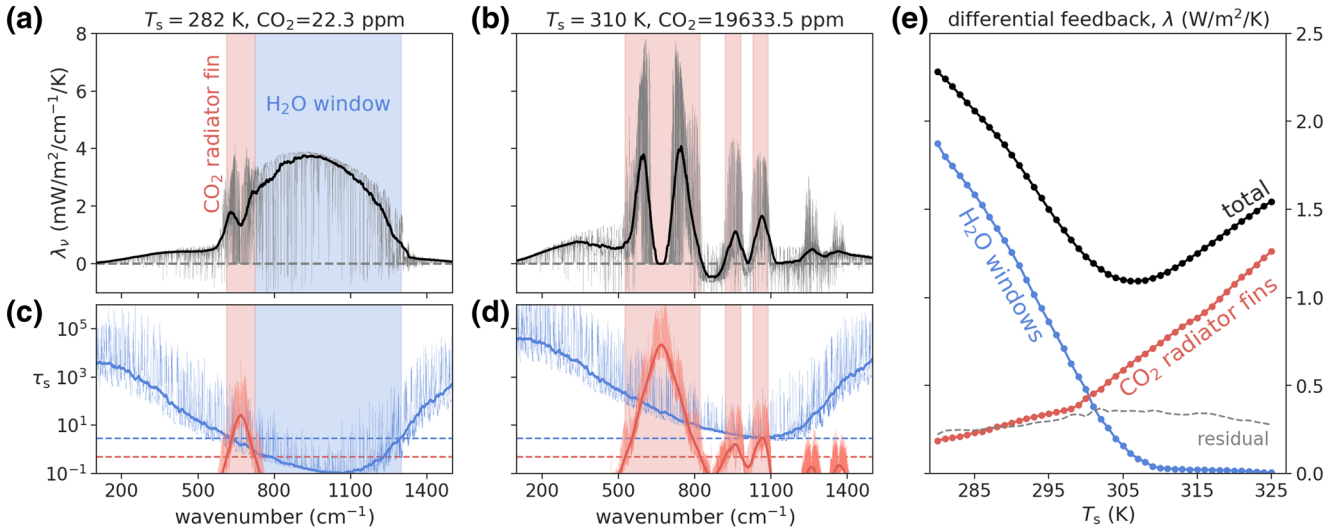

Figure 2. (a and b) Spectral differential feedbacks λ_ν (Equation 5), and (c and d) column optical depths of CO_2 and H_2O for $T_s = 282$ K (a and c) and 310 K (b and d). (e) The total differential feedback parameter λ (black), and its decomposition into contributions from H_2O windows (blue) and CO_2 radiator fins (red). These categories are defined by column optical depth thresholds (dashed lines in c and d; see the main text for details). In (a–d), the thin solid lines show results at our default spectral resolution of $\Delta\nu = 0.1$ cm^{-1}, while the thick solid lines show smoothed data (i.e., a centered mean with window width 50 cm^{-1}; for the optical depths, the mean is taken geometrically).

3.2. Spectral Feedback Analysis

We begin our spectral feedback analysis by considering the *spectral* differential feedback parameter λ_ν, defined by the spectrally resolved version of Equation 4:

$$\lambda_\nu = \frac{\mathrm{OLR}_\nu(T_s + 1, C) - \mathrm{OLR}_\nu(T_s, C)}{1\ \mathrm{K}}, \tag{5}$$

where ν denotes wavenumber (in cm^{-1}) and OLR_ν is the spectrally resolved OLR (in W/m^2/cm^{-1}). By construction, we have $\lambda = \int \lambda_\nu \, d\nu$.

In Figures 2a and 2b, we show λ_ν for $T_s = 282$ and 310 K. We focus on the wavenumber interval from 100 to 1,500 cm^{-1}, which accounts for >85% of the total feedback for all surface temperatures. Conceptually, λ_ν can be divided into three categories based on the total column optical depths of CO_2 and H_2O ($\tau_s^{CO_2}$ and $\tau_s^{H_2O}$; Figures 2c and 2d). The first category includes spectral regions within which H_2O is optically thick but CO_2 has negligible opacity (we will make these definitions precise momentarily). These spectral regions exhibit a near-zero λ_ν due to the fact that H_2O optical depths are approximately invariant functions of temperature within the atmosphere (i.e., they are independent of surface temperature; see Ingram, 2010; Jeevanjee, 2018; Jeevanjee & Romps, 2018; Koll & Cronin, 2018). We refer to this first category of wavenumbers as "Simpsonian," as the implication of T_s-invariant H_2O optical depths for OLR has been recognized since the pioneering work of Simpson (1928b). In Figures 2a and 2b, the Simpsonian spectral regions are those that have not been color-coded red or blue, corresponding to optically thick portions of the pure rotational and vibrational-rotational bands of H_2O that are not overlapped by CO_2 absorption. The fact that $\lambda_\nu \simeq 0$ in the extensive Simpsonian spectral intervals explains why water vapor significantly reduces λ compared to a pure Planck response (Ingram, 2010; Koll & Cronin, 2018).

The second category of λ_ν includes spectral regions within which H_2O is *not* optically thick, and within which CO_2 also has negligible opacity (Figures 2a and 2c, blue shading). The importance of these spectral "windows" in allowing a warmer Earth to emit more radiation to space was also recognized quite early on by Simpson (1928a). Indeed, at the cooler surface temperature of 282 K shown in Figure 2, λ_ν is nonzero primarily in the H_2O window, between ~700 and 1,300 cm^{-1}, where the increase in upwelling radiation from the surface is relatively efficiently communicated out to space. However, as can be seen by comparing λ_ν

for 282 and 310 K, as T_s increases and H_2O accumulates in the atmosphere, H_2O column opacity for a given absorption coefficient grows, and the H_2O window shrinks from the outside in. As was recently emphasized by Koll and Cronin (2018), the closing of the H_2O window counteracts the growth of λ that would otherwise result from a pure Planck response through a spectral window of fixed width. In fact by $T_s = 310$ K, the H_2O window has closed in our climate model.

Finally, the third category of λ_ν includes the spectral regions within which CO_2 does have appreciable opacity (Figure 2, red shading). For low CO_2 concentrations, this occurs only within the 15-μm band centered at 667.5 cm^{-1} (and also around 2,300 cm^{-1}, although those higher wavenumbers are not shown in Figure 2 because the reduced amplitude of the Planck function limits their importance). Because CO_2 is not a condensable gas for Earth-like temperatures, its concentration is well-mixed in the vertical, and its optical depths are *not* invariant functions of temperature within the atmosphere. In fact if one neglects the explicit temperature-scaling of absorption coefficients, CO_2 optical depths are invariant functions of *pressure* rather than temperature (Jeevanjee et al., 2020). This leads to a decidedly non-Simpsonian spectral feedback behavior in CO_2-influenced portions of the longwave spectrum.

The climate-stabilizing influence of this third spectral category is clear from the $T_s = 310$ K case depicted in Figure 2. At that surface temperature, were it not for the presence of a significant amount of CO_2 in the atmosphere, the spectral region around 15-μm would behave in the Simpsonian manner, with $\lambda_\nu \simeq 0$, due to the high opacity of H_2O there. But, because CO_2 is well-mixed and therefore does not behave in a Simpsonian manner, λ_ν exhibits prominent peaks on either side of the 15 μm band. (The spectral feedback goes to 0 at the core of the band because its emission levels are well into the isothermal stratosphere.) The evocative term "radiator fin" was introduced by Pierrehumbert (1995) to emphasize the importance of relatively dry regions of the tropics and subtropics within which the OLR is more responsive to surface warming (i.e., the local water vapor feedback in these regions is suppressed due to the climatologically low RH). Here, we use the term "CO_2 radiator fin" as a spectral analogy to this concept, to emphasize the importance of CO_2-dominated portions of the longwave spectrum in allowing OLR to increase in response to surface warming. The fact that CO_2 increases the magnitude of Earth's feedback parameter has been recognized before (Koll & Cronin, 2018; Pierrehumbert, 2010). But, as we will see, this effect becomes especially important in the absence of H_2O windows at high T_s.

To make these spectral categories precise, we first smooth the column optical depth data with a centered mean of window width 50 cm^{-1} (this mean is taken geometrically rather than arithmetically; see the thick lines in Figures 2c and 2d). Next, using this spectrally smoothed optical depth data, we (somewhat arbitrarily) define CO_2 radiator fins as having $\tau_s^{CO_2} > 0.5$, and define H_2O windows as spectral regions that are not CO_2 radiator fins and for which $\tau_s^{H_2O} < 3$. Figures 2a and 2b show that the decomposition of the spectrally resolved feedbacks according to these definitions matches by eye the different regimes exhibited by λ_ν and how they change with varying CO_2, H_2O, and T_s. With these definitions of H_2O windows and CO_2 radiator fins, we can then decompose the total λ at each T_s into the contributions from the three types of spectral regions described above. We will refer to the integral of λ_ν over H_2O windows as λ_{H_2O}, and the integral of λ_ν over CO_2 radiator fins as λ_{CO_2}.

This decomposition is shown in Figure 2e. As the surface temperature increases, the H_2O windows close, and λ_{H_2O} heads toward zero. Since λ is dominated by λ_{H_2O} at low CO_2 and T_s, λ also tracks sharply downwards for $T_s < 305$ K. At the same time, the strength of the CO_2 radiator fins increases monotonically with T_s and CO_2, and in fact λ_{CO_2} grows to dominate the total feedback by around $T_s > 305$ K. Spectral regions that do not meet the criteria for H_2O windows or CO_2 radiator fins, which are presumed to behave in an approximately Simpsonian manner, contribute a small positive feedback that is roughly constant with T_s; the small deviation from Simpsonian behavior is likely attributable to the effect of foreign-broadening on H_2O optical depths, as discussed by Ingram (2010). Thus, climate stabilization is a joint effort between λ_{H_2O} and λ_{CO_2}, with the minimum in λ (and the maximum ECS) occurring around the surface temperature at which a declining λ_{H_2O} passes the baton on to an ascending λ_{CO_2}.

The closing of the H_2O windows at high surface temperature is to be expected from the Clausius-Clapeyron scaling of water vapor path (Koll & Cronin, 2018). But what causes the strengthening of the CO_2 radiator fins? In general, the phenomenology of spectral OLR can be understood via the so-called emission-level

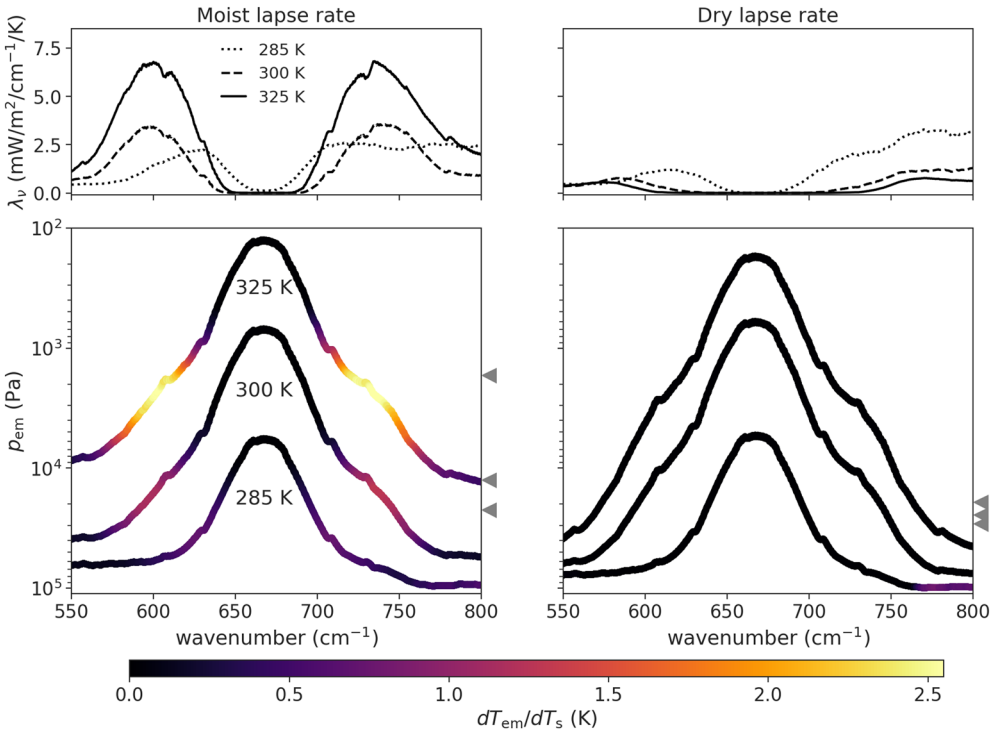

Figure 3. (Top) Smoothed λ_ν in the vicinity of 15 μm, for $T_s = 285$, 300, and 325 K. As in Figure 2, the smoothing is performed as a centered mean with window width 50 cm^{-1}. (Bottom) Smoothed emission pressures (where $\tau = \tau_{em} = 0.56$), color-coded according to the smoothed $\frac{dT_{em}}{dT_s}$. The triangles at the right of the plot mark the tropopause pressures (with high-to-low tropopause pressures corresponding to low-to-high surface temperatures). The left column shows results from the default configuration of our climate model, with a moist-adiabatic temperature profile; the right column shows results assuming a dry-adiabatic temperature profile.

(EL) approximation, which says that radiative emission to space originates from a suitably chosen emission level with optical depth τ_{em} of order unity (e.g., Jeevanjee & Fueglistaler, 2020). Within the EL framework, changes in OLR$_\nu$ with T_s (i.e., λ_ν) can then be related to changes in the *emission temperature* T_{em}, which is the temperature at which $\tau = \tau_{em}$:

$$\lambda_\nu \simeq \pi \frac{dB_\nu}{dT}\bigg|_{T_{em}} \frac{dT_{em}}{dT_s}, \tag{6}$$

where B_ν is the Planck function at wavenumber ν and $\frac{dT_{em}}{dT_s}$ is the differential change in emission temperature (relative to the surface temperature) associated with moist-adiabatic warming. The physics of Equation 6 is central to our understanding of the Simpsonian spectral intervals which we have already discussed at length: because $\tau \simeq \tau(T)$ for H_2O-dominated wavenumbers, T_{em} becomes approximately fixed once the atmosphere becomes optically thick at such wavenumbers, and thus $\frac{dT_{em}}{dT_s}$ and λ_ν are ~0. In Figure 3, we seek to better understand the strengthening of the CO_2 radiator fins through this EL framework. The left column (which we focus on here) shows results from the default configuration of our climate model, while the right column shows results from a dry-adiabatic configuration discussed in more detail in Section 3.3. All spectral data in Figure 3 smoothed with window width 50 cm^{-1}.

The top row shows λ_ν in the spectral interval centered around 15 μm for three surface temperatures that span our parameter range (285, 300, and 325 K). The lower row shows the emission pressures (i.e., the pressure at which $\tau = \tau_{em}$) for these same three surface temperatures, color-coded by $\frac{dT_{em}}{dT_s}$. We choose to define

our emission level as occurring at $\tau_{em} = 0.56$ Jeevanjee et al. (2020, Appendix B), although our results are largely unchanged as long as τ_{em} is of order unity. For each surface temperature, the tropopause pressure is marked by a triangle at the right edge of the plot.

At all values of CO_2 and T_s shown in Figure 3, the emission levels at the core of the CO_2 band occur well above the tropopause, so it is only on the wings of the CO_2 band that emission levels occur within the troposphere and can respond to the tropospheric warming. At the edges of the CO_2 band, however, where opacity from H_2O starts to dominate over opacity from CO_2, the spectral feedback again approaches zero due to the Simpsonian behavior of H_2O-dominated wavenumbers. This causes λ_ν to exhibit a twin-peaked structure. At cold surface temperatures (i.e., the 285 K case), the moist pseudoadiabat approaches the dry adiabat, so the upper-tropospheric warming is not enhanced relative to the surface. At warmer surface temperatures, however, upper-tropospheric warming is notably enhanced compared to the surface, which increases the amplitude of the twin peaks.

It can be inferred from Figure 3 that the decreasing pressure of emission levels at progressively higher CO_2 and T_s is an important ingredient of the strengthening CO_2 radiator fins. As T_s increases, the ever more amplified warming in the deepening upper troposphere occurs at ever increasing heights. If the emission levels in the CO_2 band did not keep pace with the rapidly deepening troposphere, this amplified upper-tropospheric warming would quickly become inaccessible to the CO_2 radiator fins, and their strength would be diminished. We will return to this idea in Section 3.3, in which we perform mechanism-denial tests. Note also that although increasing emission from the dominant 15-μm band alone is sufficient to produce the minimum in λ (not shown), the strengthening of CO_2 radiator fins at progressively higher CO_2 concentrations is further aided by the activation of secondary absorption bands (e.g., the band at roughly 1,000 cm^{-1} evident in Figures 2b and 2d).

While moist-adiabatic warming at fixed p sets an upper bound on $\frac{dT_{em}}{dT_s}$, in reality, two effects with the same sign cause $\frac{dT_{em}}{dT_s}$ to fall well short of the limit set by $dT/dT_s|_p$. These effects are (1) the explicit temperature-dependence of CO_2 absorption coefficients, which is important even when H_2O opacity can be neglected; and (2) overlap with H_2O opacity, which is most important at the edges of the CO_2 band (Figure S3). Unfortunately, these effects are not amenable to a simple analytical treatment, so we must use the RFM output to diagnose dT_{em}/dT_s. However, a qualitatively accurate understanding of the behavior of λ_ν within the CO_2 radiator fin is provided by combining enhanced upper-tropospheric warming on a moist adiabat with a progressively deepening CO_2 emission peak.

3.3. Mechanism-Denial Tests

Figure 2 shows that the existence of the minimum in λ, and the resulting peak in ECS, results from the strengthening of the CO_2 radiator fins and the closing of the H_2O windows. To test this conclusion, we performed several mechanism-denial tests to prevent various aspects of the relevant physics from playing their role in establishing the λ minimum.

We first repeated our calculations without including the H_2O continuum within the wavenumber interval from 700 to 1,200 cm^{-1}, in which case the H_2O window does not close even at the highest surface temperatures we consider, and the total feedback parameter remains large across our parameter range (Figure 4, left). Therefore, due to the monotonically increasing F_{2x}, ECS increases monotonically with T_s in this no-continuum configuration of our model. Next, we modified our climate model to use a dry-adiabatic lapse rate in the troposphere instead of the moist pseudoadiabat. Since warming on a dry adiabat is not enhanced in the upper troposphere, this change prevents the rapid warming of the CO_2 emission levels at high surface temperature, which is a key ingredient of the strengthening of the CO_2 radiator fins at high CO_2 and T_s (Figure 3, second column). As a result, in this case the total feedback parameter tracks the dwindling strength of the H_2O windows, and there is no minimum in λ (Figure 4, left). This behavior is expected in a traditional "runaway" scenario, where the OLR becomes decoupled from the surface temperature (e.g., Nakajima et al., 1992). Therefore, we see that moist convection (i.e., the establishment of a moist-adiabatic

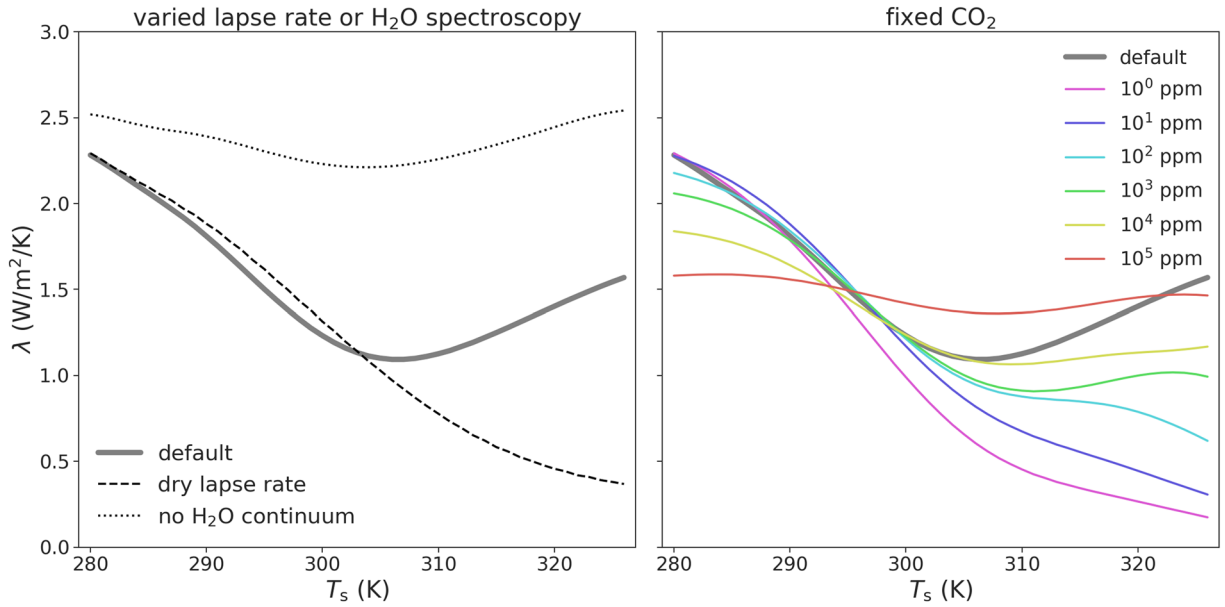

Figure 4. (Left) A comparison of the differential feedback parameter λ for the default configuration of our climate model, a version that assumes a dry-adiabatic troposphere, and a version that neglects H_2O continuum opacity between 700 and 1,200 cm^{-1} in the radiative transfer calculations. (Right) A comparison of λ calculated with varying fixed amounts of CO_2 instead of the energetically consistent varying amount of CO_2 at each T_s.

troposphere) stabilizes the system against the possibility of a runaway in comparison to a climate system with a dry-adiabatic troposphere. Similar results were also obtained in Lindzen et al. (1982).

As can be inferred from Figure 3, the strengthening of the CO_2 radiator fins at high T_s is also dependent on the energetically consistent increase of CO_2 with T_s. We explore this further in the right panel of Figure 4 by recalculating λ as a function of T_s but with fixed amounts of CO_2. For small amounts of CO_2 (100 ppm or less), the deepening upper troposphere outgrows the CO_2 emission levels at high T_s, preventing the strengthening of the CO_2 radiator fins. As a result, λ decreases monotonically as a function of T_s for small CO_2 inventories, although the approach to zero (the runaway limit) is delayed by adding more CO_2 (consistent with the analysis of Koll and Cronin [2018]). At higher CO_2 concentrations (1,000 ppm or more), there is a very shallow minimum in λ. Even this shallow minimum in λ all but disappears for a constant, very high concentration of CO_2 of 10^5 ppm.

In summary, these mechanism-denial tests have shown that the ECS peak in our climate model depends on (1) an H_2O continuum to quickly close the windows; (2) moist-adiabatic tropospheric temperatures to provide enhanced upper-tropospheric warming; and (3) a progressively deepening CO_2 peak to take full advantage of (2).

4. Discussion

We have demonstrated here a longwave, clear-sky mechanism for the ECS peak around T_s = 310 K. Although the physics on which our mechanism depends is present in models across the hierarchy, more work is needed to establish whether this mechanism indeed governs the ECS peak seen in comprehensive climate models. The peak ECS value in our model (about 5.5 K) is slightly smaller in magnitude than the median value reported in previous work (6–8 K), and significantly smaller than the largest values (>15 K) reported by Wolf et al. (2018) and Popp et al. (2016). To further investigate whether our clear-sky longwave mechanism can explain a larger ECS peak magnitude, we reran our calculations with the radiation calculated by the Rapid Radiative Transfer Model (RRTM; Mlawer et al., 1997), a correlated-*k* code, instead of by the RFM. We found that the magnitude of the ECS peak increased to >8 K (Figure S3). Therefore, it is possible that differences in radiative transfer modeling could account for some of the spread in ECS peak values.

Shortwave feedbacks, which we have neglected here, are also sure to play a role in setting the magnitude of the ECS peak. A further complication is that comprehensive models exhibit a radiative-convective transition

around T_s = 310 K, where the closing of the water vapor window causes net radiative heating rather than cooling in the atmospheric boundary layer. This changes the structure of the boundary layer and low clouds (Popp et al., 2016; Wolf & Toon, 2015; Wordsworth & Pierrehumbert, 2013), which could also amplify or modulate the ECS peak studied here. Further work, likely involving mechanism-denial experiments across a model hierarchy (Jeevanjee et al., 2017), will be needed to determine which mechanisms dominate.

Since our mechanism for the ECS peak is a thermodynamically driven minimum in the climate feedback parameter, this mechanism may be relevant to the sensitivity of Earth's climate to other types of forcing. Indeed, numerous studies of insolation-driven warming have found a region of increased *specific* climate sensitivity (essentially the inverse of λ_{eff}, with units of K/W/m^2) at surface temperatures between roughly 310 and 320 K (Gómez-Leal et al., 2018, 2019; Leconte et al., 2013; Wolf & Toon, 2015). However, the results shown in the right panel of our Figure 4 cast some doubt on the relevance of our mechanism to the insolation scenario: when we warm our model at fixed CO_2 (as would occur due to increasing insolation), we do not obtain an appreciable minimum (maximum) in the feedback parameter (specific climate sensitivity). Again, further tests with more comprehensive models are required to clarify the extent to which the climate sensitivity peaks in CO_2-driven and insolation-driven warming have a common cause.

Even if the longwave clear-sky mechanism discussed here does not dominate in comprehensive models, the results of this paper nonetheless help shed new light on climate feedbacks. For instance, the spectral feedback decomposition shown in Figure 2 yields a new perspective on climate sensitivity, which would be difficult to glean from the more conventional Planck + water vapor + lapse rate decomposition. In particular, the λ_{CO_2} component highlights the climate-stabilizing role of the non-Simpsonian CO_2 "radiator fins," especially in combination with moist-adiabatic upper-tropospheric warming (Figure 3).

Further study of λ_{CO_2} could also clarify the possibility of CO_2-induced runaway greenhouse states. Previous studies in an astronomical context are often focused on habitability and so do not equilibrate CO_2 concentrations with T_s at a fixed insolation (e.g., Goldblatt et al., 2013; Kasting et al., 1993; Ramirez et al., 2014; Wordsworth & Pierrehumbert, 2013). For equilibrated, CO_2-driven warming, however, the results shown here suggest that the *increase* in CO_2 with increasing T_s yields a constantly strengthening CO_2 radiator fin which is able to keep climate stable up to relatively high CO_2 and T_s (consistent with the results of Boschi et al., 2013). Further work could test this idea by pushing CO_2 and T_s to much higher values than those considered here. Such efforts would need to incorporate shortwave radiative transfer, because for very large CO_2 inventories, the enhanced planetary albedo from enhanced Rayleigh scattering would effectively decrease the F_{2x} inferred from longwave-only calculations (Forget et al., 2013). This effect would presumably further stabilize the climate against a CO_2-induced runaway.

Data Availability Statement

The data and source code used to make the figures appearing in this manuscript are available at https://doi.org/10.5281/zenodo.4298573.

Acknowledgments
The authors thank Daniel Koll and an anonymous reviewer for their helpful feedback on this manuscript. The radiative transfer model used in this work (the RFM) is available from its author, Anu Dudhia (Anu.Dudhia@physics.ox.ac.uk), upon request.

References

Arrhenius, S. (1896). On the influence of carbonic acid in the air upon the temperature of the ground. *Philosophical Magazine Series*, *41*(251), 237–276. https://doi.org/10.1080/14786449608620846

Bloch-Johnson, J., Pierrehumbert, R. T., & Abbot, D. S. (2015). Feedback temperature dependence determines the risk of high warming. *Geophysical Research Letters*, *42*, 4973–4980. https://doi.org/10.1002/2015GL064240

Boschi, R., Lucarini, V., & Pascale, S. (2013). Bistability of the climate around the habitable zone: A thermodynamic investigation. *Icarus*, *226*(2), 1724–1742. https://doi.org/10.1016/j.icarus.2013.03.017

Caballero, R., & Huber, M. (2013). State-dependent climate sensitivity in past warm climates and its implications for future climate projections. *Proceedings of the National Academy of Sciences of the United States of America*, *110*(35), 14162–14167. https://doi.org/10.1073/pnas.1303365110

Clough, S. A., Iacono, M. J., & Moncet, J.-L. (1992). Line-by-line calculations of atmospheric fluxes and cooling rates: Application to water vapor. *Journal of Geophysical Research*, *97*(D14), 15761. https://doi.org/10.1029/92JD01419

Cousin, C., Le Doucen, R., Boulet, C., & Henry, A. (1985). Temperature dependence of the absorption in the region beyond the 4.3-μm band head of CO_2. 2: N_2 and O_2 broadening. *Applied Optics*, *24*(22), 3899. https://doi.org/10.1364/AO.24.003899

Dudhia, A. (2017). The reference forward model (RFM). *Journal of Quantitative Spectroscopy and Radiative Transfer*, *186*, 243–253. https://doi.org/10.1016/j.jqsrt.2016.06.018

Forget, F., Wordsworth, R., Millour, E., Madeleine, J. B., Kerber, L., Leconte, J., et al. (2013). 3D modelling of the early martian climate under a denser CO_2 atmosphere: Temperatures and CO_2 ice clouds. *Icarus*, *222*(1), 81–99. https://doi.org/10.1016/j.icarus.2012.10.019

Goldblatt, C., Robinson, T. D., Zahnle, K. J., & Crisp, D. (2013). Low simulated radiation limit for runaway greenhouse climates. *Nature Geoscience*, *6*(8), 661–667. https://doi.org/10.1038/ngeo1892

Gómez-Leal, I., Kaltenegger, L., Lucarini, V., & Lunkeit, F. (2018). Climate sensitivity to carbon dioxide and the moist greenhouse threshold of Earth-like planets under an increasing solar forcing. *The Astrophysical Journal*, *869*(2), 129. https://doi.org/10.3847/1538-4357/aaea5f

Gómez-Leal, I., Kaltenegger, L., Lucarini, V., & Lunkeit, F. (2019). Climate sensitivity to ozone and its relevance on the habitability of Earth-like planets. *Icarus*, *321*, 608–618. https://doi.org/10.1016/j.icarus.2018.11.019

Gordon, I., Rothman, L., Hill, C., Kochanov, R., Tan, Y., Bernath, P., et al. (2017). The HITRAN2016 molecular spectroscopic database. *Journal of Quantitative Spectroscopy and Radiative Transfer*, *203*, 3–69. https://doi.org/10.1016/J.JQSRT.2017.06.038

Hartmann, D. L., & Larson, K. (2002). An important constraint on tropical cloud-climate feedback. *Geophysical Research Letters*, *29*(20), 1951. https://doi.org/10.1029/2002GL015835

Ingram, W. J. (2010). A very simple model for the water vapour feedback on climate change. *Quarterly Journal of the Royal Meteorological Society*, *136*(646), 30–40. https://doi.org/10.1002/qj.546

IPCC. (2014). *Observations: Ocean pages. Climate change 2013—The physical science basis* (pp. 255–316). https://doi.org/10.1017/CBO9781107415324.010

Jeevanjee, N. (2018). *The physics of climate change: Simple models in climate science*. arxiv preprint. Retrieved from http://arxiv.org/abs/1802.02695

Jeevanjee, N., & Fueglistaler, S. (2020). On the cooling-to-space approximation. *Journal of the Atmospheric Sciences*, *77*(2), 465–478. https://doi.org/10.1175/JAS-D-18-0352.1

Jeevanjee, N., Hassanzadeh, P., Hill, S., & Sheshadri, A. (2017). A perspective on climate model hierarchies. *Journal of Advances in Modeling Earth Systems*, *9*, 1760–1771. https://doi.org/10.1002/2017MS001038

Jeevanjee, N., & Romps, D. M. (2018). Mean precipitation change from a deepening troposphere. *Proceedings of the National Academy of Sciences of the United States of America*, *115*(45), 11465–11470. https://doi.org/10.1073/pnas.1720683115

Jeevanjee, N., Seeley, J. T., Paynter, D. J., & Fueglistaler, S. (2020). An analytical model for spatially varying clear-sky CO_2 forcing. *Earth*. arXiv preprint. https://www.essoar.org/doi/abs/10.1002/essoar.10500379.1

Kasting, J. F., Whitmire, D. P., & Reynolds, R. T. (1993). Habitable zones around main sequence stars. *Icarus*, *101*, 108–128.

Kluft, L., Dacie, S., Buehler, S. A., Schmidt, H., & Stevens, B. (2019). Re-examining the first climate models: Climate sensitivity of a modern radiative–convective equilibrium model. *Journal of Climate*, *32*(23), 8111–8125. https://doi.org/10.1175/JCLI-D-18-0774.1

Knutti, R., & Rugenstein, M. A. (2015). Feedbacks, climate sensitivity and the limits of linear models. *Philosophical Transactions of the Royal Society A: Mathematical, Physical and Engineering Sciences*, *373*(2054). https://doi.org/10.1098/rsta.2015.0146

Knutti, R., Rugenstein, M. A., & Hegerl, G. C. (2017). Beyond equilibrium climate sensitivity. *Nature Geoscience*, *10*(10), 727–736. https://doi.org/10.1038/NGEO3017

Koll, D. D. B., & Cronin, T. W. (2018). Earth's outgoing longwave radiation linear due to H_2O greenhouse effect. *Proceedings of the National Academy of Sciences of the United States of America*, *115*(41), 10293–10298. https://doi.org/10.1073/pnas.1809868115

Leconte, J., Forget, F., Charnay, B., Wordsworth, R., & Pottier, A. (2013). Increased insolation threshold for runaway greenhouse processes on Earth-like planets. *Nature*, *504*(7479), 268–271. https://doi.org/10.1038/nature12827

Lindzen, R. S., Hou, A. Y., & Farrell, B. F. (1982). The role of convective model choice in calculating the climate impact of doubling CO_2. *Journal of Atmospheric Sciences*, *39*, 1189–1205.

Manabe, S., & Strickler, R. F. (1964). Thermal equilibrium of the atmosphere with a convective adjustment. *Journal of the Atmospheric Sciences*, *21*(4), 361–385. https://doi.org/10.1175/1520-0469(1964)021⟨0361:TEOTAW⟩2.0.CO;2

Meraner, K., Mauritsen, T., & Voigt, A. (2013). Robust increase in equilibrium climate sensitivity under global warming. *Geophysical Research Letters*, *40*, 5944–5948. https://doi.org/10.1002/2013GL058118

Mlawer, E. J., Payne, V. H., Moncet, J.-L., Delamere, J. S., Alvarado, M. J., & Tobin, D. C. (2012). Development and recent evaluation of the MT_CKD model of continuum absorption. *Philosophical Transactions of the Royal Society A: Mathematical, Physical and Engineering Sciences*, *370*(1968), 2520–2556. https://doi.org/10.1098/rsta.2011.0295

Mlawer, E. J., Taubman, S. J., Brown, P. D., Iacono, M. J., & Clough, S. A. (1997). Radiative transfer for inhomogeneous atmospheres: RRTM, a validated correlated-k model for the longwave. *Journal of Geophysical Research*, *102*(D14), 16663. https://doi.org/10.1029/97JD00237

Nakajima, S., Hayashi, Y.-Y., & Abe, Y. (1992). A study on the "runaway greenhouse effect" with a one-dimensional radiative–convective equilibrium model.*Journal of Atmospheric Sciences*, *49* (23), 2256–2266. https://doi.org/10.1175/1520-0469(1992)049⟨2256:ASOTGE⟩2.0.CO;2

Pierrehumbert, R. T. (1995). Thermostats, radiator fins, and the local runaway greenhouse. *Journal of Atmospheric Sciences*, *52*(10), 1784–1806. https://doi.org/10.1175/1520-0469(1995)052⟨1784:TRFATL⟩2.0.CO;2

Pierrehumbert, R. T. (2010). *Principles of planetary climate*. Cambridge, UK: Cambridge University Press. Retrieved from https://books.google.com/books?hl=en&lr=&id=bO_U8f5pVR8C&pgis=1

Popp, M., Schmidt, H., & Marotzke, J. (2016). Transition to a moist greenhouse with CO_2 and solar forcing. *Nature Communications*, *7*, 10627. https://doi.org/10.1038/ncomms10627

Ramirez, R. M., Kopparapu, R. K., Lindner, V., & Kasting, J. F. (2014). Can increased atmospheric CO_2 levels trigger a runaway greenhouse? *Astrobiology*, *14*(8), 714–731. https://doi.org/10.1089/ast.2014.1153

Rohling, E. J., Sluijs, A., Dijkstra, H. A., Köhler, P., Van De Wal, R. S., Von Der Heydt, A. S., et al. (2012). Making sense of palaeoclimate sensitivity. *Nature*, *491*(7426), 683–691. https://doi.org/10.1038/nature11574

Romps, D. M. (2020). Climate sensitivity and the direct effect of carbon dioxide in a limited-area cloud-resolving model. *Journal of Climate*, *33*(9), 3413–3429. https://doi.org/10.1175/jcli-d-19-0682.1

Russell, G. L., Lacis, A. A., Rind, D. H., Colose, C., & Opstbaum, R. F. (2013). Fast atmosphere-ocean model runs with large changes in CO_2. *Geophysical Research Letters*, *40*, 5787–5792. https://doi.org/10.1002/2013GL056755

Seeley, J. T., Jeevanjee, N., & Romps, D. M. (2019). FAT or FiTT: Are anvil clouds or the tropopause temperature-invariant? *Geophysical Research Letters*, *46*, 1842–1850. https://doi.org/10.1029/2018gl080096

Sherwood, S. C., Webb, M. J., Annan, J. D., Armour, K. C., Forster, P. M., Hargreaves, J. C., et al. (2020). An assessment of Earth's climate sensitivity using multiple lines of evidence. *Reviews of Geophysics*, *58*, e2019RG000678. https://doi.org/10.1029/2019rg000678

Simpson, G. (1928a). Further studies in terrestrial radiation. *Monthly Weather Review*, *56*(8), 322–323. https://doi.org/10.1175/1520-0493(1928)56⟨322:FSITR⟩2.0.CO;2

Simpson, G. (1928b). Some studies in terrestrial radiation. *Memoirs of the Royal Meteorological Society*, *2*(16), 69–95.
Wolf, E. T., Haqq-Misra, J., & Toon, O. B. (2018). Evaluating climate sensitivity to CO_2 across Earth's history. *Journal of Geophysical Research: Atmospheres*, *123*, 11861–11874. https://doi.org/10.1029/2018JD029262
Wolf, E. T., & Toon, O. B. (2015). The evolution of habitable climates under the brightening Sun. *Journal of Geophysical Research: Atmospheres*, *120*, 5775–5794. https://doi.org/10.1002/2015JD023302
Wordsworth, R. D., & Pierrehumbert, R. T. (2013). Water loss from terrestrial planets with CO_2-rich atmospheres. *The Astrophysical Journal*, *778*(2), 154. https://doi.org/10.1088/0004-637X/778/2/154
Zhong, W., & Haigh, J. D. (2013). The greenhouse effect and carbon dioxide. *Weather*, *68*(4), 100–105. https://doi.org/10.1002/wea.2072